Experimental study on residual stress in high-speed grinding of noncircular equidistant profile

Wei Liu (lw1986tiger@163.com)
Hunan University of Science and Technology
Houcai Yuan
Xinyu Shi
Tao Liu
Shishuai Du

Research Article

Keywords: noncircular equidistant profile, high-speed grinding, X-C axis linkage, grinding temperature, surface roughness, residual stress

Posted Date: April 25th, 2022

DOI: https://doi.org/10.21203/rs.3.rs-1563403/v1

Abstract

To explore the formation mechanism of residual stress in the high-speed grinding of noncircular equidistant profile, the orthogonal experiments were designed with three grinding parameters including the grinding wheel speed, workpiece speed and grinding depth. A ceramic bond CBN grinding wheel was used for the high-speed grinding of noncircular equidistant profile by the X-C axis linkage. The effects of the three grinding parameters on the grinding temperature, surface roughness and residual stress were analyzed. The results show that with the increase of grinding wheel speed, the grinding temperature and residual stress increase, and the surface roughness decreases. As the increase of workpiece speed, the grinding temperature and residual stress decrease, and the surface roughness increases. As the increase of grinding depth, the grinding temperature, residual stress and surface roughness increase. Besides, the grinding depth has the greatest influence on the residual stress, followed by the grinding wheel speed and workpiece speed.

1. Introduction

With the continuous designing optimization of mechanical structure, higher requirements of performance for the mechanical component are put forward. To improve the connection and transmission performance of mechanical parts, the structure of noncircular equidistant profile is derived. For the precision machining of profile axis, the high-speed grinding is usually used to ensure the forming quality. However, the coupling effect of force and heat in the grinding process has an important effect on the residual stress[1]. It is generally considered that the residual compressive stress after grinding is beneficial to the surface quality of parts, which can increase the closing force of microcracks, hinder the crack propagation and prolong the fatigue life. The residual tensile stress is harmful, which will reduce the tensile yield limit and fatigue strength of workpiece, and accelerate the fatigue failure [2].

Many researchers have studied the influence of grinding parameters, such as the grinding wheel speed (v_s), workpiece speed (v_w) and grinding depth (a_p), on the residual stress. Zhang et al. [3] found an approximate linear growth between the surface residual stress of 45 steel and the grinding depth through wet grinding. For the surface wet grinding of n-WC/12Co coating surface, Deng et al. [4] found that the residual compressive stress increased with the increase of grinding depth and workpiece speed. For the AISI1010 steel coated with WC-10Co-4Cr, Zoei et al. [5] found that the residual compressive stress increased with the decrease of grinding wheel speed. Wang et al. [6] studied the residual stress of EA4T steel by the surface dry grinding. With the increase of workpiece speed, the residual tensile stress on the surface decreased first and then increased; with the increase of grinding depth and grinding wheel speed, the residual tensile stress increased. Wang et al. [7] and Zhang et al. [8] studied the cylindrical dry grinding of carburized carbon steel 18CrNiMo7-6, and found that the residual stress was compressive stress. Azarhoushang et al. [9] found that a significant reduction in the workpiece temperature was realized when the grinding wheel was 60 percent structured, and it could greatly reduce the residual tensile stress. For

the multistage cylindrical wet grinding of AISI 4140, Florian et al. [10] found that the pre-grinding combined with grind-strengthening could obtain a stable and high residual compressive stress.

Most scholars believe that the grinding temperature is the main cause of residual tensile stress, then the controlling method for residual tensile stress is mainly to control the grinding temperature. Li et al. [11] proposed a novel approach of regulating the residual stress during the induction heating assisted grinding, which made the temperature distribution uniform, thereby diminished the residual tensile stress. For the surface wet grinding of FGH96, Wang et al. [12] found that the grinding temperature could not reach the critical value of thermoplastic deformation, and then the surface residual stress was mainly the compressive stress generated by the cold plastic deformation. Dražumerič et al. [13] developed a new temperature-based method for the feed increment of crankshaft grinding, and found that it could avoid thermal damage, such as tensile residual stress. Silva et al. [14] found that the wet grinding could reduce the residual tensile stress caused by the grinding thermal action, and showed a residual compressive stress. Choudhary et al. [15] studied the effect of minimum quantity lubrication (MQL) on the brittle material surface in the high-speed grinding, and found that the cold plastic deformation was increased and the friction was reduced, thus led to the higher residual compressive stress. Zhao et al. [16] explored the distribution of grinding temperature and the rule of residual stress by the tree-shaped root profile grinding. Soga et al. [18] found that the grinding residual stress for the ductile iron was tensile. Deng et al. [19] found that the residual compressive stress and surface roughness for 3Y-TZP increased with an increase in the grinding depth or a decrease in the grinding wheel speed.

Above all, the researches of grinding residual stress were mainly on the surface grinding and cylindrical grinding. Therefore, it is necessary to explore the formation mechanism of residual stress in the high-speed grinding of noncircular equidistant profile. The orthogonal experiments with three factors and four levels were carried out to study the effects of grinding wheel speed, workpiece speed and grinding depth on the grinding temperature, surface roughness and residual stress.

2. Experimental Methods And Systems

2. 1 Material

As shown in Fig. 1 (a), the workpiece is the noncircular equidistant profile shaft used in the mining hoist winch reducer, and the material is 45 steel after carburizing and quenching. The tensile strength is 600 MPa, the yield strength is 355 MPa, and the Brinell hardness is 229 HBS.

The workpiece dimension is shown in Fig. 1 (b), and the length of profile section is 70 mm, which is selected for the grinding experiment. The cross-section of the profile is show in Fig. 1 (c). The radius r_j is 26.87 mm, the dividing circle radius r_f is 22.39 mm, the radius r_x is 10.61 mm, and the radius r_d is 49.39 mm.

2. 2 Experimental methods

According to the characteristics of noncircular equidistant profile, as shown in Fig. 1, the X-C axis linkage grinding was selected. The X-C axis linkage grinding is accomplished by the feed of X-axis and the rotation of C-axis. The motion principle is shown in Fig. 2. The expression for the noncircular equidistant profile is defined as $\rho = OP = \rho(\theta)$. Take point J as the grinding starting point, point P as any current grinding point, the rotation angle of grinding point is $\angle JOP = \theta$, while the actual rotation angle is $\angle JOO_2 = \alpha$. The radius of grinding wheel is r_s, and the radius of basic circle is r_j. The grinding wheel moves along the X-axis in the horizontal direction and rotates around O_2, and the model of X-C axis linkage is:

$$\begin{cases} X(\theta) = \sqrt{\overline{OP}^2 + r_s^2 - 2\overline{OP} \cdot r_s \cdot \cos(\pi - \varphi)} - r_j - r_s \\ C = \alpha = \theta - (\arctan\left(\dfrac{\overline{OM}}{\overline{OP}}\right) - \arctan\left(\dfrac{\overline{ON}}{\overline{O_2N}}\right)) \end{cases} \quad (1)$$

By taking the first derivative of grinding wheel displacement $X(\theta)$, the X-axis feed speed of grinding wheel can be calculated. The date calculated by this model was programmed into the CNC grinding machine.

2. 3 Experimental system

As shown in Fig. 3 (a), a composite grinder CNC8325 was selected to carry out the X-C axis linkage high-speed grinding. A ceramic bond CBN grinding wheel was used, whose concentration was 175, and the particle size was 120#. A diamond wheel was selected for the grinding dressing.

As a noncircular workpiece, it is difficult to measure the grinding temperature of the whole workpiece surface using thermocouple thermometry. Therefore, the grinding temperature was measured by an infrared thermograph FLIR-SC325, as shown in Fig. 3 (b). The infrared thermograph was set to a measurement range of 20-1200 °C. The residual stress was measured by a residual stress analyzer HP-MK2, which was mainly composed by the punching equipment, microscope and resistance strain gauge, as shown in Fig. 3 (c). The surface roughness of workpiece was detected by a roughness tester TR200, as shown in Fig. 4 (a). The surface topography of workpiece was observed by a microsystem VHX-500FE, as shown in Fig. 4 (b).

The experimental parameters for the dry up-grinding are shown in Table 1. As the grinding wheel speed, workpiece speed and grinding depth were independent with each other, the interactive influence was not considered. Accordingly, a $L_{16}(4^3)$ standard orthogonal array was obtained to design the experiments, as listed in Table 2.

Table 1 Experimental parameters

Parameters	Values
Grinding wheel speed, v_s(m/s)	60,80,100,120
Workpiece speed, v_w(r/min)	30,50,70,90
Grinding depth, a_p(μm)	10,20,30,40

3. Results And Discussion

For each experiment, the grinding temperature, surface roughness, minimum and maximum residual stresses are shown in Table 2.

Table 2 Orthogonal experiment schedule and results

NO.	Grinding wheel speed v_s(m/s)	Workpiece speed v_w(r/min)	Grinding depth a_p (μm)	Grinding temperature (°C)	Surface roughness Ra (μm)	Min-Residual Stress (MPa)	Max-Residual Stress (MPa)
1	60	30	10	361. 2	1.81	69	189
2	60	50	30	764. 6	2.30	81	230
3	60	70	20	570. 3	2.41	61	145
4	60	90	40	760. 8	3.14	79	197
5	80	30	20	620. 5	2.31	83	185
6	80	50	40	860. 4	2.15	90	248
7	80	70	30	654. 9	2.51	82	258
8	80	90	10	366. 5	2.57	55	151
9	100	30	30	770. 9	2.24	94	208
10	100	50	10	367. 1	2.45	77	204
11	100	70	40	827. 3	2.27	98	284
12	100	90	20	600. 2	2.52	85	253
13	120	30	40	910. 7	2.54	117	374
14	120	50	20	560. 4	2.27	96	301
15	120	70	10	447. 3	2.23	72	176
16	120	90	30	757. 4	1.71	87	235

3. 1 Effect of grinding wheel speed

The effect of grinding wheel speed on the grinding result is shown in Fig.5. The grinding temperature increased with the increase of grinding wheel speed. As the grinding wheel speed increased, the number of effective abrasive grains per unit time that involved in the grinding increased, the friction and cutting effect between abrasive grains and workpiece increased, and the heat generated by the friction and thermoplastic deformation of workpiece increased. Although much heat was taken away by the generated chips, the speed of heat propagation in the workpiece surface was large than the grinding speed, and a large amount of grinding heat entered into the workpiece, making the grinding temperature rise.

As shown in Fig. 5, the surface roughness decreased with the increasing grinding wheel speed. Firstly, as the grinding wheel speed increased, the maximum undeformed chip thickness and grinding force decreased, resulting in a decrease in the surface roughness. Secondly, as the grinding wheel speed increased, the number of effective abrasive grains per unit time that involved in grinding increased; then the degree of interference between scratches increased, and the workpiece surface became smoother, resulting in a smaller surface roughness.

For dry grinding, the tensile stress caused by the grinding heat was greater than the compressive stress caused by the mechanical extrusion. As shown in Fig. 5, both the minimum and maximum residual stresses were tensile stresses, and they increased with the increase of grinding wheel speed, while the growth rate of maximum residual stress was slightly higher than that of the minimum residual stress. During the high-speed grinding, the residual tensile stress was mainly affected by the grinding thermal action. The higher the grinding temperature, the greater the residual tensile stress produced.

3. 2 Effect of workpiece speed

The effect of workpiece speed on the grinding result is shown in Fig. 6. The grinding temperature decreased with the increase of workpiece speed, and the decreasing rate became more and more gentle. As the workpiece speed increased, the grinding contact time in a unit contact region decreased, and the number of effective abrasive grains that involved in the grinding decreased, then the grinding heat decreased and the grinding temperature gradually decreased.

As shown in Fig. 6, the surface roughness increased with the increase of workpiece speed. Firstly, as the workpiece speed increased, the maximum undeformed chip thickness and grinding force increased, resulting in an increase in the surface roughness. Secondly, as the workpiece speed increased, the grinding contact time in a unit contact region decreased, resulting in a larger surface roughness.

As shown in Fig. 6, the minimum and maximum residual stresses decreased with the increase of workpiece speed. The decreasing rate of maximum residual tensile stress was greater than that of the minimum residual tensile stress. As the workpiece speed increased, the grinding contact time in a unit

contact region decreased, and the compressive stress caused by the mechanical extrusion increased, the tensile stress caused by the grinding heat decreased. As the workpiece speed increased from 70 r/min to 90 r/min, the decreasing rate of grinding temperature became small, the influence of grinding thermal stress decreased, and the mechanical extrusion stress increased, then the maximum residual tensile stress decreased rapidly.

3. 3 Effect of grinding depth

The influence of grinding depth on the grinding result was shown in Fig. 7. The grinding temperature increased with the increase of grinding depth, and the increase rate was gradually gentle. As the grinding depth increased, the contact arc length between the grinding wheel and workpiece increased, and the number of effective abrasive grains that involved in grinding increased, then the energy transferred to the workpiece increased, resulting in an increase in the grinding temperature. With the increase of grinding depth, the chip volume and heat taken away by the chips increased, but the heat taken away by the chips could not exceed the melting energy, resulting in a slow increase rate in the grinding temperature.

As shown in Fig. 7, the surface roughness increased with the increase of grinding depth. As the grinding depth increased, the material removal rate and grinding force increased, and the maximum undeformed chip thickness increased, resulting in an increase in the surface roughness.

As shown in Fig. 7, both the minimum and maximum residual stresses increased with the increase of grinding depth. When the grinding depth exceeded 30 μm, the grinding temperature exceeded the A_{c1} temperature of 45 steel, and the martensite of body-centered cubic lattice transformed into the austenite of face-centered cubic lattice, which reduced the volume of workpiece material. For the bound deformation of internal material, additional residual tensile stress due to the phase transformation eventually generated on the surface. Therefore, the increase rate of residual tensile stress increased, when the increase rate of grinding temperature decreased. Grinding burns would be generated when the grinding temperature was higher than the A_{c1} of workpiece material, which should be avoided.

3.4 Topography

The typical ground surface topographies are shown in Fig. 8, which are corresponding to the experiments of no. 3, no. 4, no. 8, no. 16 respectively. For the experiment of no. 3, the maximum residual stress was the lowest, which was 145 MPa. For the experiment of no. 4, the surface scratches were obvious and mixed, while the surface roughness was the highest, and the ground surface topography was the worst for the maximum workpiece speed and grinding depth. For the experiment of no. 13, the grinding temperature was the highest, and the ground surface topography was better for the maximum grinding wheel speed. For the experiment of no. 16, the surface roughness was the lowest, and the ground surface was even and delicate, without obvious machining defects and burn marks.

3.5 Comprehensive discussion

By the variance analysis for each grinding characteristic in Table 2, Fig. 9 obtained. The grinding depth was the most influential factor for the grinding temperature and residual stress, followed by the grinding wheel speed and workpiece speed. The grinding depth was also the most influential factor for the surface roughness, but followed by the workpiece speed and grinding wheel speed. Combined with Fig. 5, Fig. 6 and Fig. 7, it was found that the effects of grinding wheel speed and grinding depth on the residual stress were positively correlated, but the effect of workpiece speed on the residual stress was negatively correlated.

4. Conclusion

The noncircular equidistant profile was processed by the high-speed grinding of X-C axis linkage, and the effects of grinding parameters on the grinding temperature, surface roughness and residual stress were analyzed. The following conclusions were obtained:

- Within the range of experimental parameters, the grinding temperature and residual stress were positively correlated with the grinding wheel speed and grinding depth, and negatively correlated with the workpiece speed. The surface roughness increased with the increase of workpiece speed and grinding depth, and decreased with the increase of grinding wheel speed.
- The variation trend of residual stress was basically consistent with that of the grinding temperature, which indicated that the residual tensile stress was greatly affected by the grinding heat.
- The effects of grinding wheel speed and workpiece speed on the surface roughness and residual stress were opposite. The essence was the change of the number of abrasive grains involved in the grinding. Therefore, the grinding wheel speed and workpiece speed can be appropriately selected to control the surface roughness and residual stress.

Therefore, in the high-speed grinding of noncircular equidistant profile experiment, a higher grinding wheel speed can be used to obtain a lower surface roughness, and a higher workpiece speed can be used to obtain a lower residual tensile stress. Simultaneously, a moderate grinding depth can be used to ensure a better surface quality.

Declarations

Ethical Approval

This article has not been published or submitted elsewhere.

Authors contributions

Wei Liu developed the idea for the study, Xinyu Shi, Houcai Yuan, Tao Liu and Shishuai Du did the analyses, Houcai Yuan and Wei Liu wrote the paper.

Competing interests

The authors declare no conflict of interest.

Availability of data and materials

The authors confirm that the data and materials supporting the findings of this study are available within the article.

Acknowledgement

The authors would like to thank the Scientific Research Fund of Hunan Provincial Education Department (Grants no. 20A202), Natural Science Foundation of Hunan Province (Grant no. 2020JJ5178 and 2020JJ4024) and Open Foundation of Hunan Provincial Key Laboratory of High Efficiency and Precision Machining of Difficult-to-Cut Material (Grant no. E21849) for the financial support.

References

1. Mahdi M, Zhang LC (1999) Applied mechanics in grinding. part 7: residual stress induced by the all coupling of mechanical deformation, thermal deformation and phase transformation. Int J Mach Tool Manuf 39: 1285-1298. https://doi.org/10.1016/S0890-6955(98)00094-7
2. Ding WF, Zhang LC, Li Z, Zhu YJ. et al (2017) Review on grinding-induced residual stresses in metallic materials. Int J Adv Manuf Technol 88, 2939–2968. https://doi. org/10.1007/s00170-016-8998-1
3. Zhang XM, Xiu SC, Shi XL, Liu MH (2014) Influence of small depth cut on grinding surface micro-structure damage and mechanism. J Northeast Univ (Nat Sci) 35(7): 1010-1014. doi:10.12068/j.issn.1005-3026.2014.07.022
4. Deng ZH, Jin Q, An L (2008) Finite-element simulation and experiment on the residual stress when grinding nanostructured WC/12Co coatings. Journal of Mechanical Engineering 44(7): 58-62. https://doi.org/10.3321/j.issn:0577-6686.2008.07.009
5. Zoei MS, Sadeghi MH, Salehi M (2016) Effect of grinding parameters on the wear resistance and residual stress of HVOF-deposited WC–10Co–4Cr coating. Surf Coat Technol 307: 886-891. https://doi.org/10.1016/j.surfcoat.2016.09.067
6. Wang CY, Zhao J, Zhu HW, Zheng QQ, Sun QZ (2018) Effect of grinding parameters on grinding residual stress of EA4T steel. Scientific and Technological Innovation (32): 22-23. https://doi.org/10.3969/j.issn.1673-1328.2018.32.010
7. Wang D, Wang JJ, Li L (2020) Study on surface integrity of cylindrical grinding 18CrNiMo7-6. Journal of Chongqing Institute of Technology 34(4): 76-86. https://doi.org/10.3969/j.issn.1674-8425(z).2020.04.010
8. Zhang YX, Yang X, Yuan SS, Zhu JH, Wang D (2021) Residual stress of high-speed cylindrical grinding of 18CrNiMo7-6 steel. China Mechanical Engineering 32(5): 540-546. https://doi.org/10.3969/j.issn.1004-132X.2021.05.005

9. Azarhoushang B, Daneshi A, Lee DH (2017) Evaluation of thermal damages and residual stresses in dry grinding by structured wheels. J Cleaner Prod 142: 1922-1930. https://doi.org/10.1016/j.jclepro.2016.11.091
10. Florian B, Heiner M, Carsten H, Daniel M, Jérémy E (2020) Development of surface residual stress and surface state of 42CrMo4 in multistage grinding. Procedia CIRP 87(C): 198-203. https://doi.org/10.1016/j.procir.2020.02.095
11. Li F, Li XK, Wang T, Rong YM, Steven LY (2020) In-process residual stresses regulation during grinding through induction heating with magnetic flux concentrator. Int J Mech Sci 172: 105393. https://doi.org/10.1016/j.ijmecsci.2019.105393
12. Wang ZM, Wang HN, Li X, Yu JH, Xu RF (2020) Surface Integrity of Powder Metallurgy Superalloy FGH96 Affected by Grinding with Electroplated CBN Wheel. Procedia CIRP 87(C): 204-209. https://doi.org/10.1016/j.procir.2020.02.101
13. Dražumerič R, Roininen R, Badger J, Krajnik P (2018) Temperature-based method for determination of feed increments in crankshaft grinding. J Mater Process Technol 259: 228-234. https://doi.org/10.1016/j.jmatprotec.2018.04.032
14. da Silva LR, da Silva DA, dos Santos FV. et al (2019) Study of 3D parameters and residual stress in grinding of AISI 4340 steel hardened using different cutting fluids. Int J Adv Manuf Technol 100: 895–905. https://doi.org/10.1007/s00170-018-2763-6
15. Choudhary A, Naskar A, Paul S (2018) Effect of minimum quantity lubrication on surface integrity in high-speed grinding of sintered alumina using single layer diamond grinding wheel. Ceram Int 44: 17013-17021. https://doi.org/10.1016/j.ceramint.2018.06.144
16. Zhao ZC, Qian N, Ding WF, Wang Y, Fu YC (2020) Profile grinding of DZ125 nickel-based super alloy: Grinding heat, temperature field, and surface quality. J Manuf Prosess 57: 10-22. https://doi.org/10.1016/j.jmapro.2020.06.022
17. Anderson D, Warkentin A, Bauer R (2008) Comparison of numerically and analytically predicted contact temperatures in shallow and deep dry grinding with infrared measurements. Int J Mach Tools Manuf 48(3–4): 320–328. https://doi.org/10.1016/j.ijmachtools.2007.10.010
18. Sosa AD, Echeverría MD, Moncada OJ, Sikora JA (2007) Residual stresses, distortion and surface roughness produced by grinding thin wall ductile iron plates. Int J Mach Tools Manuf 47(2): 229-235. https://doi.org/10.1016/j.ijmachtools.2006.04.004.
19. Deng XS, Zhang FL, Liao YL, Bai FH, Li KJ, Zhou YM, Wu SH, Wang CY (2022) Effect of grinding parameters on surface integrity and flexural strength of 3Y-TZP ceramic. Journal of the European Ceramic Society 42(4): 1635-1644. https://doi.org/10.1016/j.jeurceramsoc.2021.12.018.

Figures

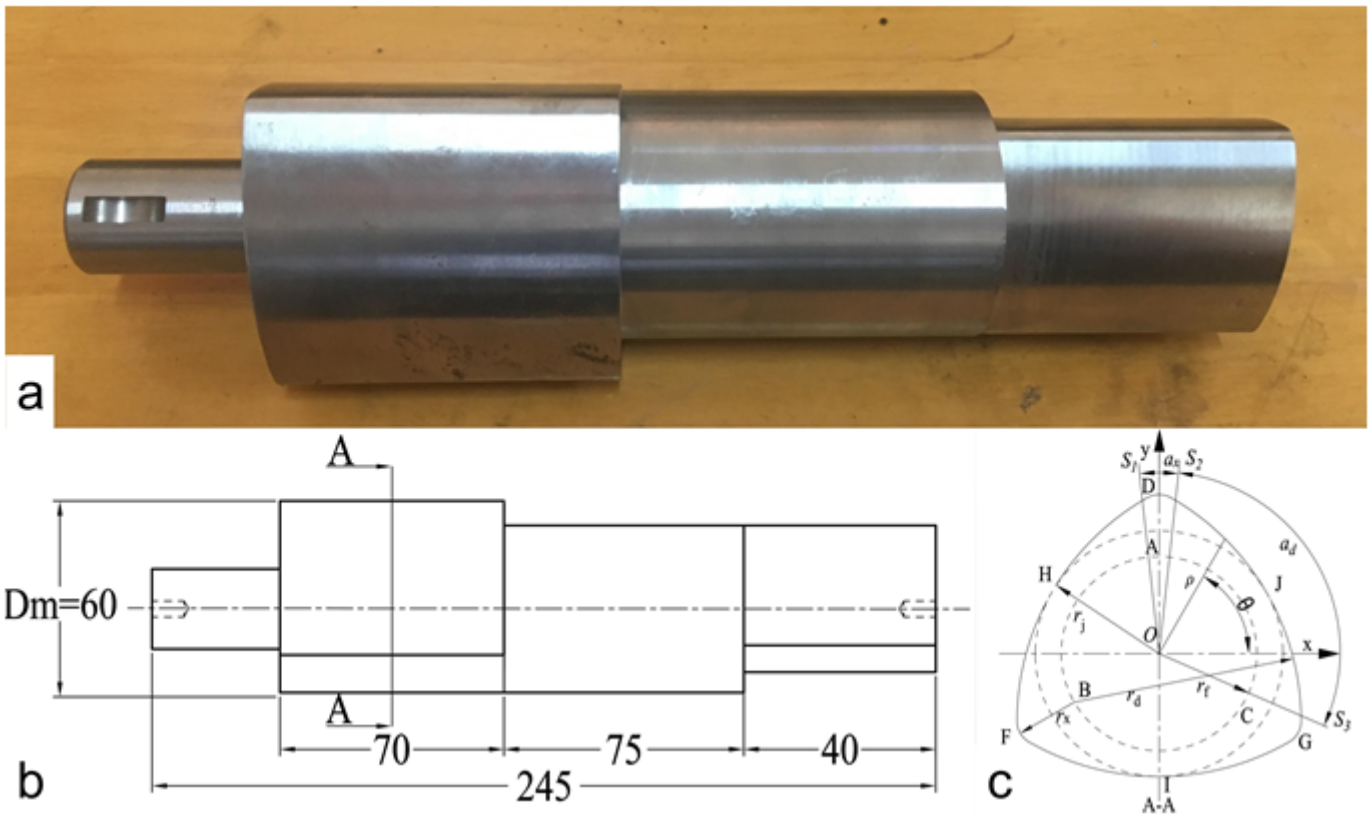

Figure 1

Workpiece: (a) Real workpiece (b) Workpiece dimension (c) Noncircular equidistant profile

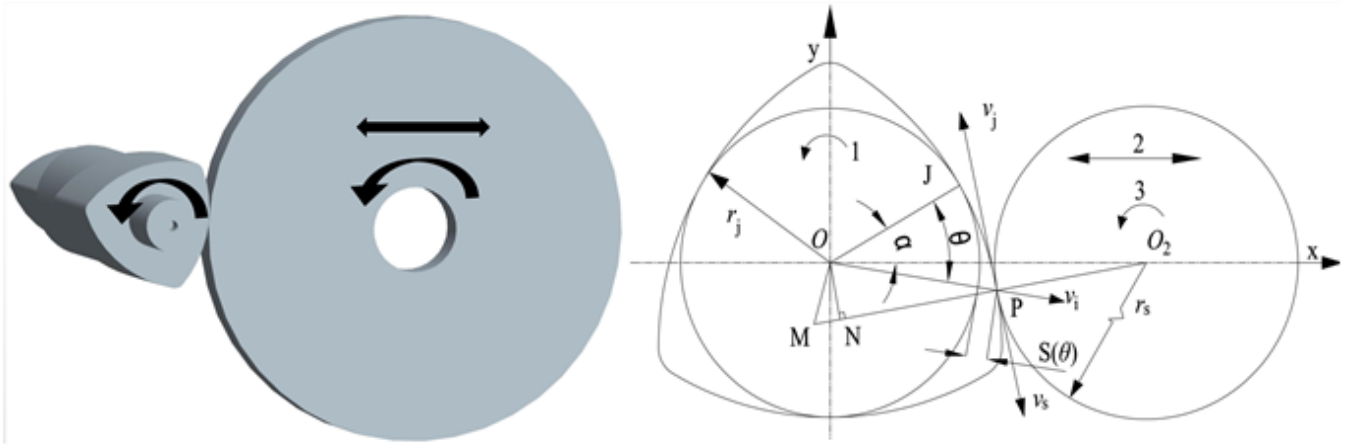

Figure 2

X-C axis linkage grinding model

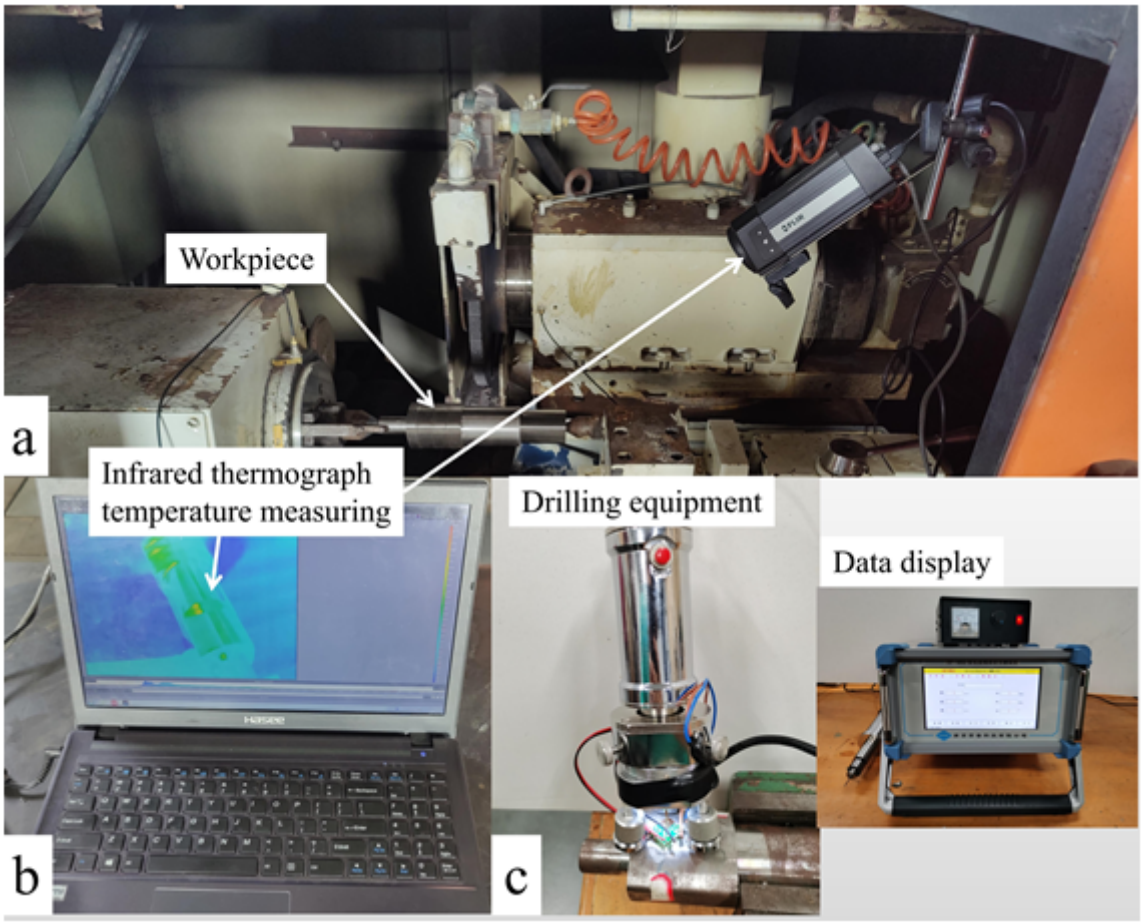

Figure 3

Experimental system: (a) High-speed grinder (b) Infrared thermograph measurement (c) Residual stress measurement

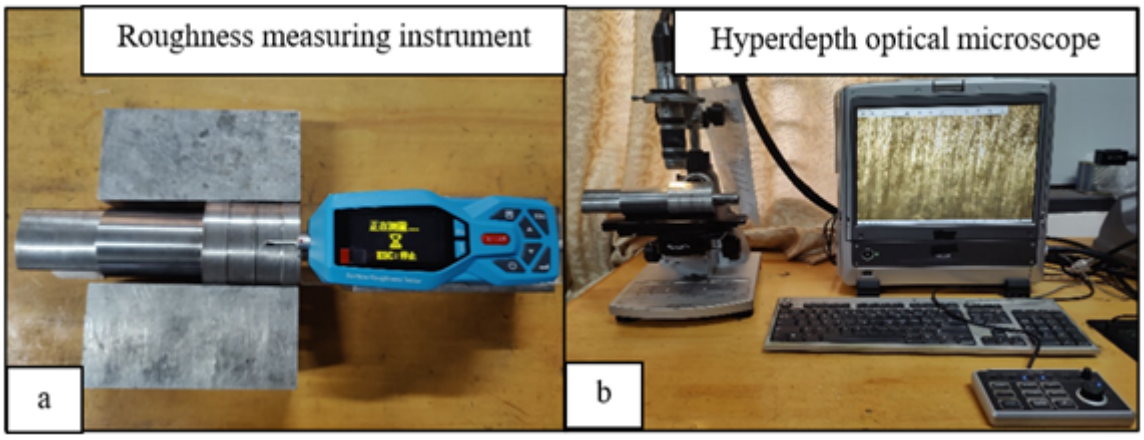

Figure 4

Measuring apparatus: (a) Roughness tester (b) Microscope

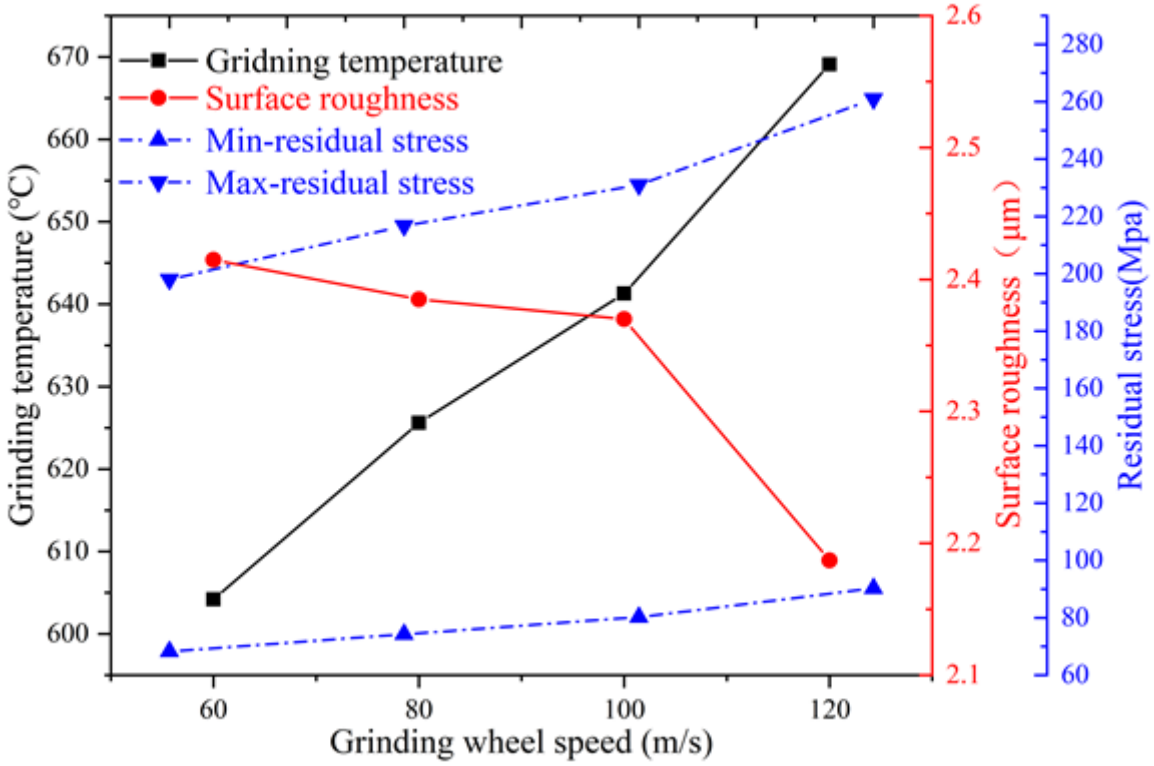

Figure 5

Effect of grinding wheel speed

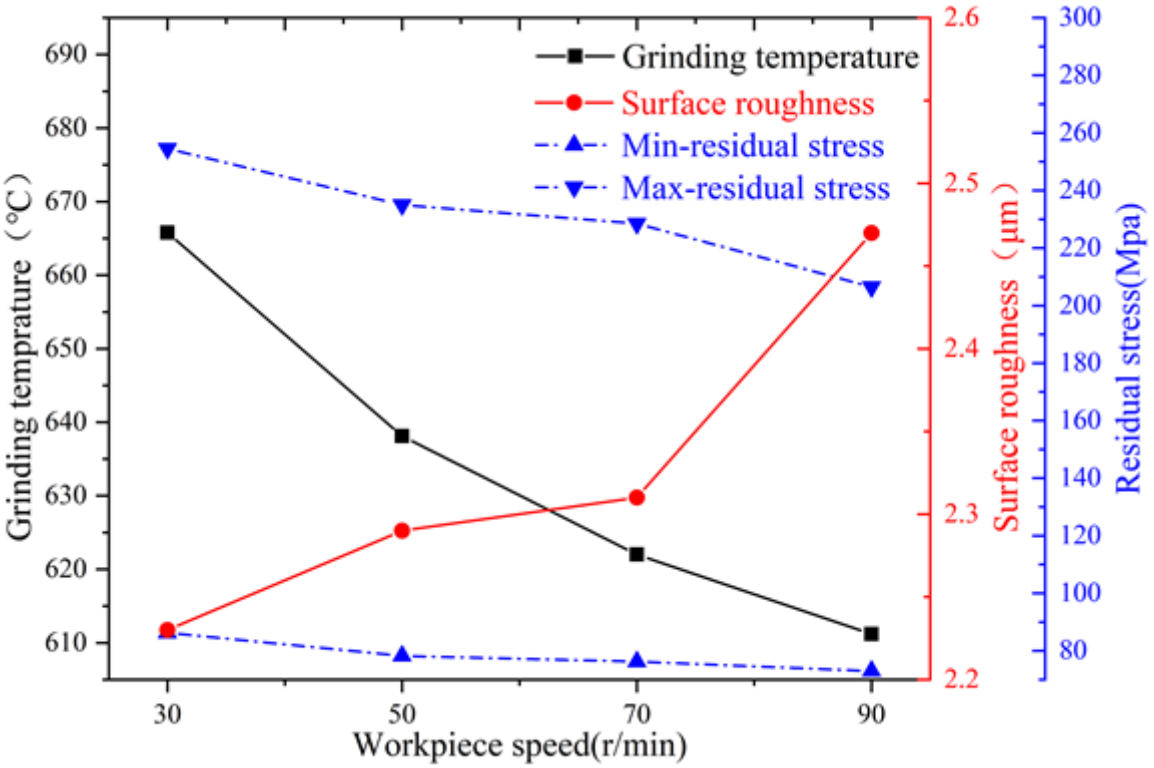

Figure 6

Effect of workpiece speed

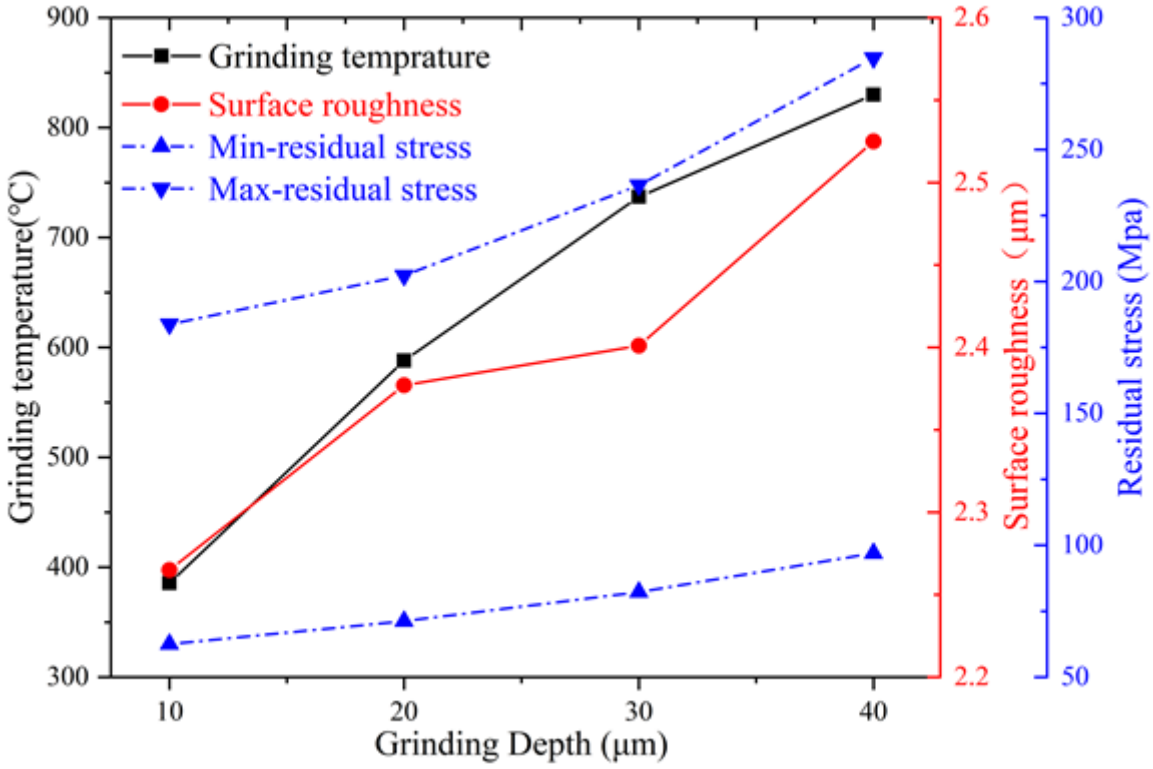

Figure 7

Effect of grinding depth

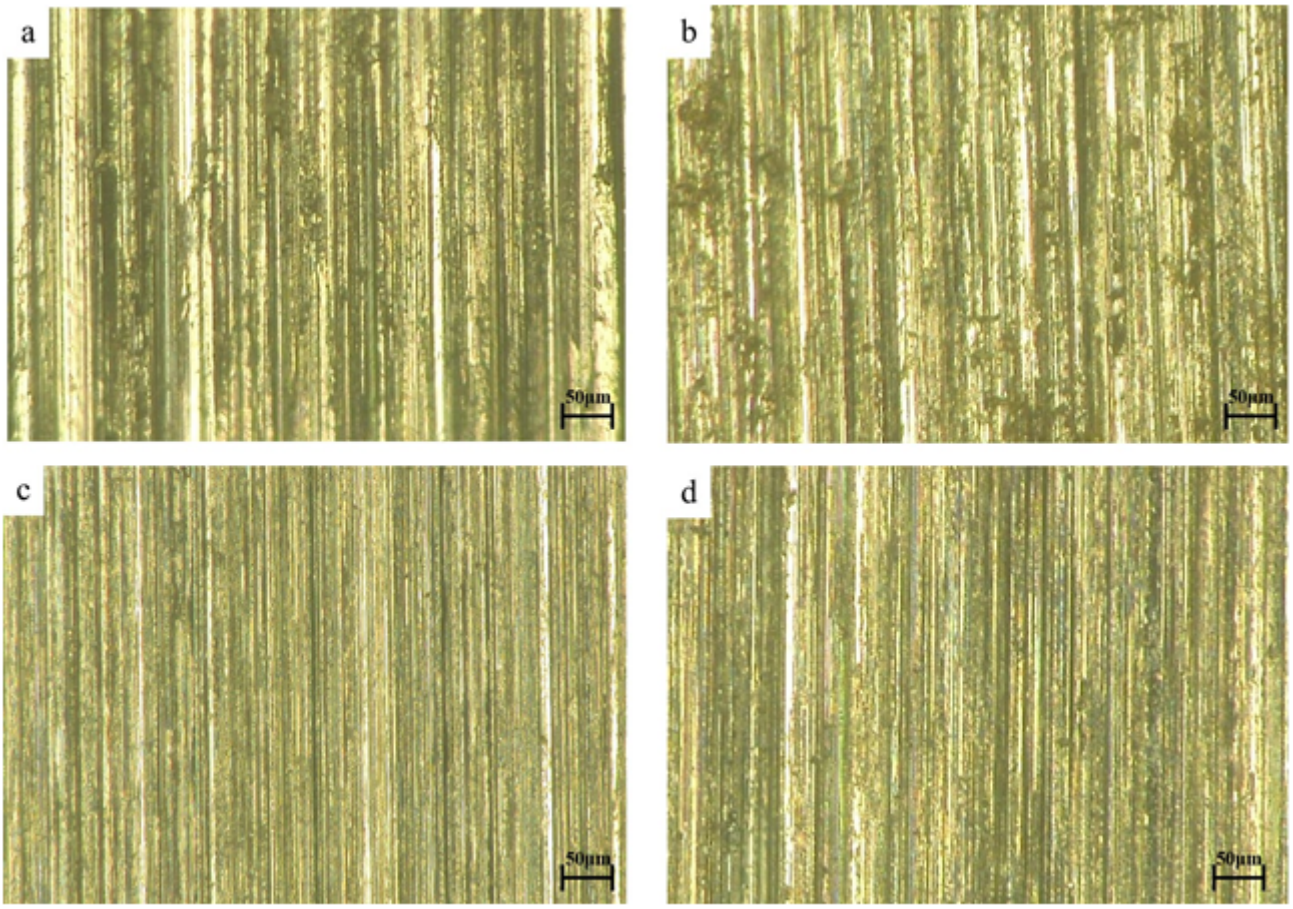

Figure 8

Workpiece surface topography: (a) Experiment no. 3 (b) Experiment no. 4 (c) Experiment no. 13 (d) Experiment no. 16

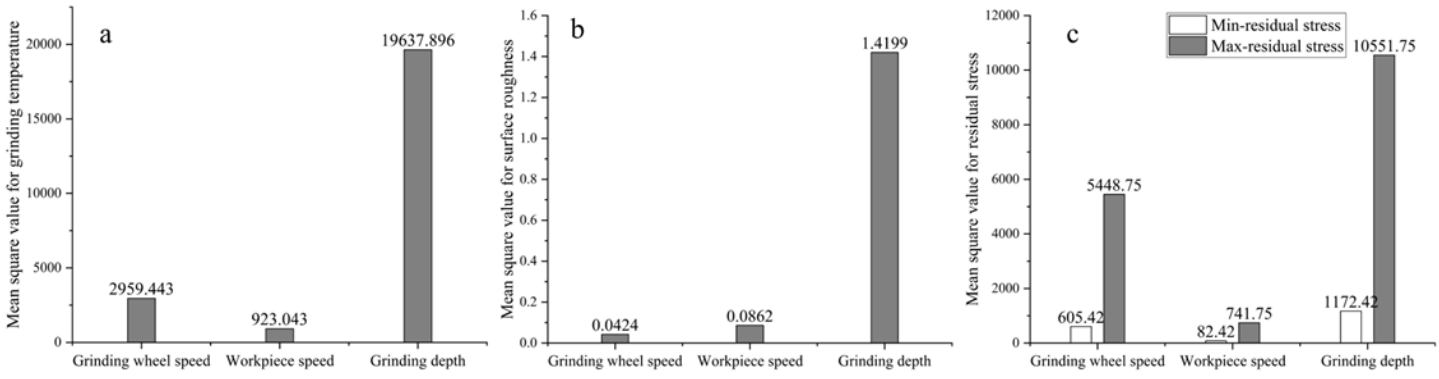

Figure 9

The mean square value by variance analysis: (a) Grinding temperature (b) Surface roughness (c) Residual stress